Iranian Journal of Science (2023) 47:1843–1859
https://doi.org/10.1007/s40995-023-01531-6

RESEARCH PAPER

Mg-Dopant Effects on Band Structures of Zn-Based Hydroxyapatites: A Theoretical Study

Niyazi Bulut[1] · Omer Kaygili[1] · Ala Hamd Hssain[1,2] · Sergey V. Dorozhkin[3] · Benahmed Abdelghani[4] · Cahit Orek[1] · Hanifi Kebiroglu[1] · Tankut Ates[5] · Rebaz Obaid Kareem[2]

Received: 31 March 2023 / Accepted: 28 September 2023 / Published online: 25 October 2023

Abstract
The band structures of Zn-based hydroxyapatites co-doped with Mg at varying amounts from 0 to 2.0 at. % have been investigated theoretically in more detail. The calculations were done to obtain the band structure, density of states, and band gap for all the modeled structures to study their electronic properties. It was seen that the co-doping has an effect on the structural and electronic properties of all the as-investigated structures. The bandgap energy for all samples in each group was found to be reduced gradually with varying doping rates of Mg into Zn-doped HAp. The band gap decreased from 4.54 to 3.84 eV for samples of 0.4Zn–0.4 Mg-HAp and 2.0Zn–0.4 Mg-HAp with the same amount of Mg, respectively, as a result of increasing the doping levels of Zn from 0.4 to 2.0 at.%. The lattice parameters, unit cell volume, and density decrease with increase in doping of Zn-containing HAp and in addition of second dopant Mg at varying amounts 0.4, 0.8, 1.2, 1.6, and 2.0 at. % in all of the modeled sample group. Furthermore, it is observed that the declining values of the aforementioned parameters are significantly impacted by the increasing Zn doping rates.

Keywords Hydroxyapatite · Density functional theory · Band gap

1 Introduction

Hydroxyapatite (HAp) is one of the most significant and extensively used bioceramics. As well as its non-toxic properties, HAp has superior bioactivity and biocompatibility because it has chemical and structural similarities with the mineral phase of mammalian bones and teeth; therefore, HAp has been widely employed in bone tissue engineering, drug delivery, orthopedics, and dentistry (Sun et al. 2014; Yin et al. 2014; Liao et al. 2014). HAp has a hexagonal structure with $P6_3/m$ or $P6_3$ space group as well as the stoichiometric composition $Ca_{10}(PO_4)_6(OH)_2$ (Fig. 1). For the hexagonal HAp, the lattice parameters are $a = b = 0.9418$ nm and $c = 0.6884$ nm. As shown in Fig. 1, Ca ions can be located in the unit cell at two distinct sites: Ca(I) and Ca (II). The crucial characteristics of HAp include the Ca/P molar ratio of 1.667 (Kaygili et al. 2015).

Because of its unique crystal structure and chemical makeup, HAp is easy to dope with various ions. Ca deficiency of HAp can also be the result of defect introduction. The stability, morphology, solubility, mechanical characteristics, and biological behaviors of HAp might be changed by doping ions and introducing defects into the crystal lattice (Koutsopoulos 2002). Numerous experiments have been performed on HAp with other elements like magnesium, iron, copper, zinc, and strontium (Bhattacharjee et al. 2019; Coelho et al. 2019; Ullah et al. 2018). Due to its poor mechanical characteristics, HAp usage as an implant material in medical fields appears to be challenging. To obtain a stronger mechanical property, several chemical elements are added to pure HAp as dopants (Badran et al.

✉ Omer Kaygili
okaygili@firat.edu.tr

[1] Department of Physics, Faculty of Science, Firat University, 23119 Elazig, Turkey

[2] Physics Department, College of Science, University of Halabja, Halabja, Iraq

[3] Kudrinskaja square, 1-155, Moscow, Russia 123242

[4] Department of Physics, Faculty of Science, University of Dr. Moulay Tahar, Saida Algeria, Algeria

[5] Department of Engineering Basic Sciences, Faculty of Engineering and Natural Sciences, Malatya Turgut Özal University, Battalgazi, Malatya, Turkey

2017; Kaygili et al. 2013). Namely, metal ions of iron, copper, cobalt, and zinc were doped to HAp at 0.5 wt. %, 1.0 wt. %, and 1.5 wt. %. The introduction of these metals into such pure HAp occurs for a variety of reasons. Owing to iron's ability to boost the magnetic facility of pure HAp, artificial bone grafts may be produced from Fe-doped HAp,

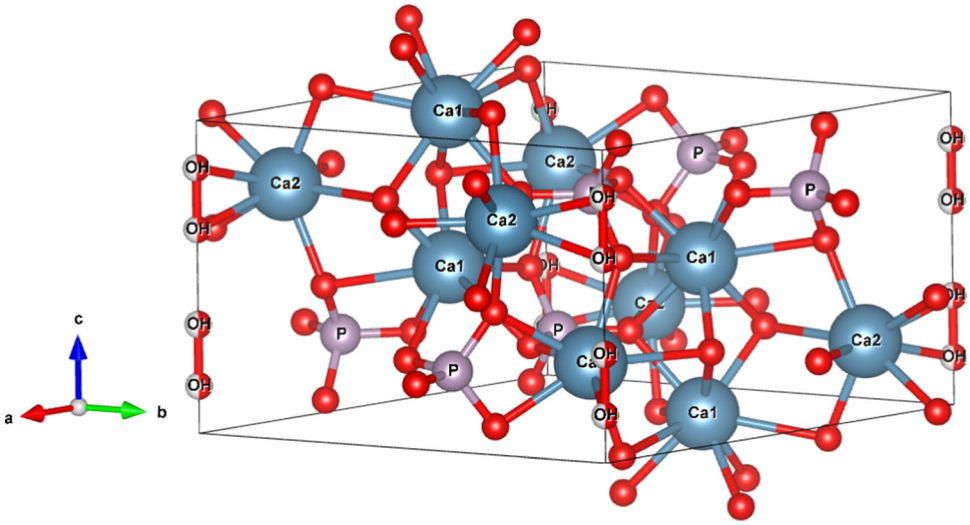

Fig. 1 The optimized geometry belonging to the HAp. Here, the red balls represent oxygen atoms

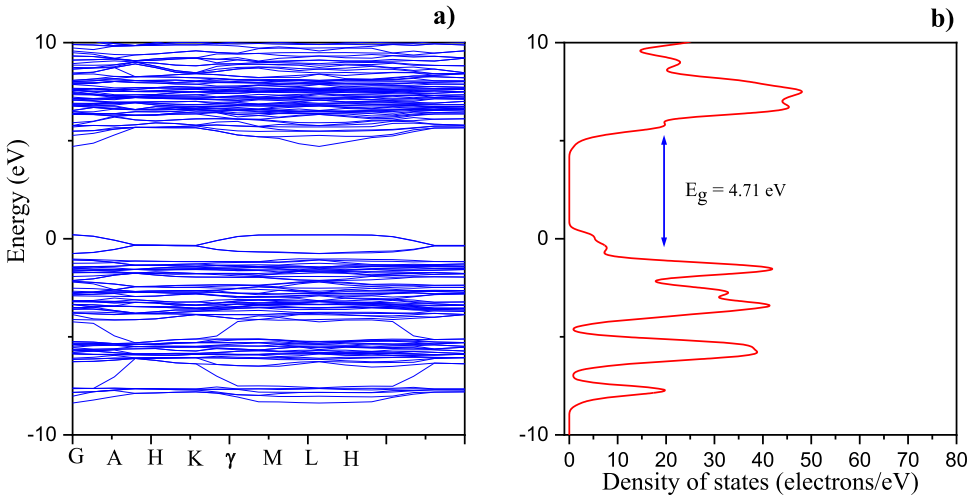

Fig. 2 **a** The band structure and **b** density of states for the pure HAp (Mahmood et al. 2020)

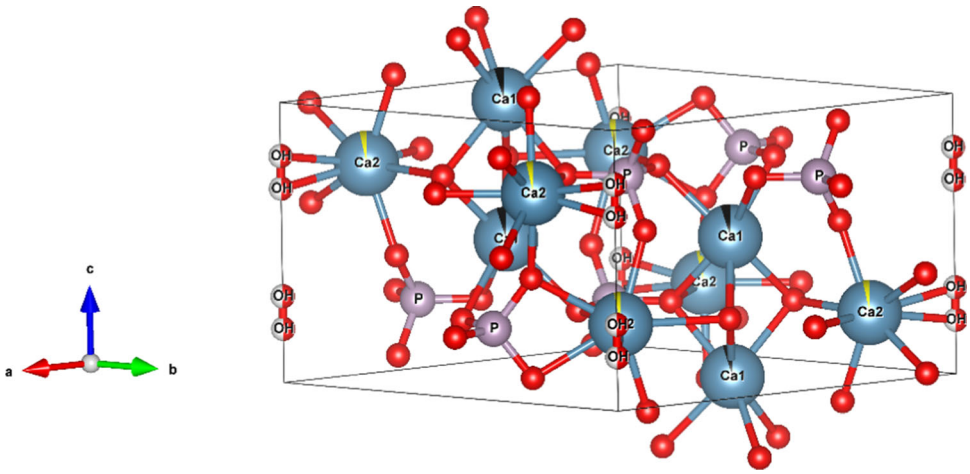

Fig. 3 The optimized geometry belonging to the 2.0Zn–2.0 Mg-HAp (the red balls represent oxygen atoms, and yellow (Mg) and black (Zn) fractions are symbolized the occupied regions in the Ca sites)

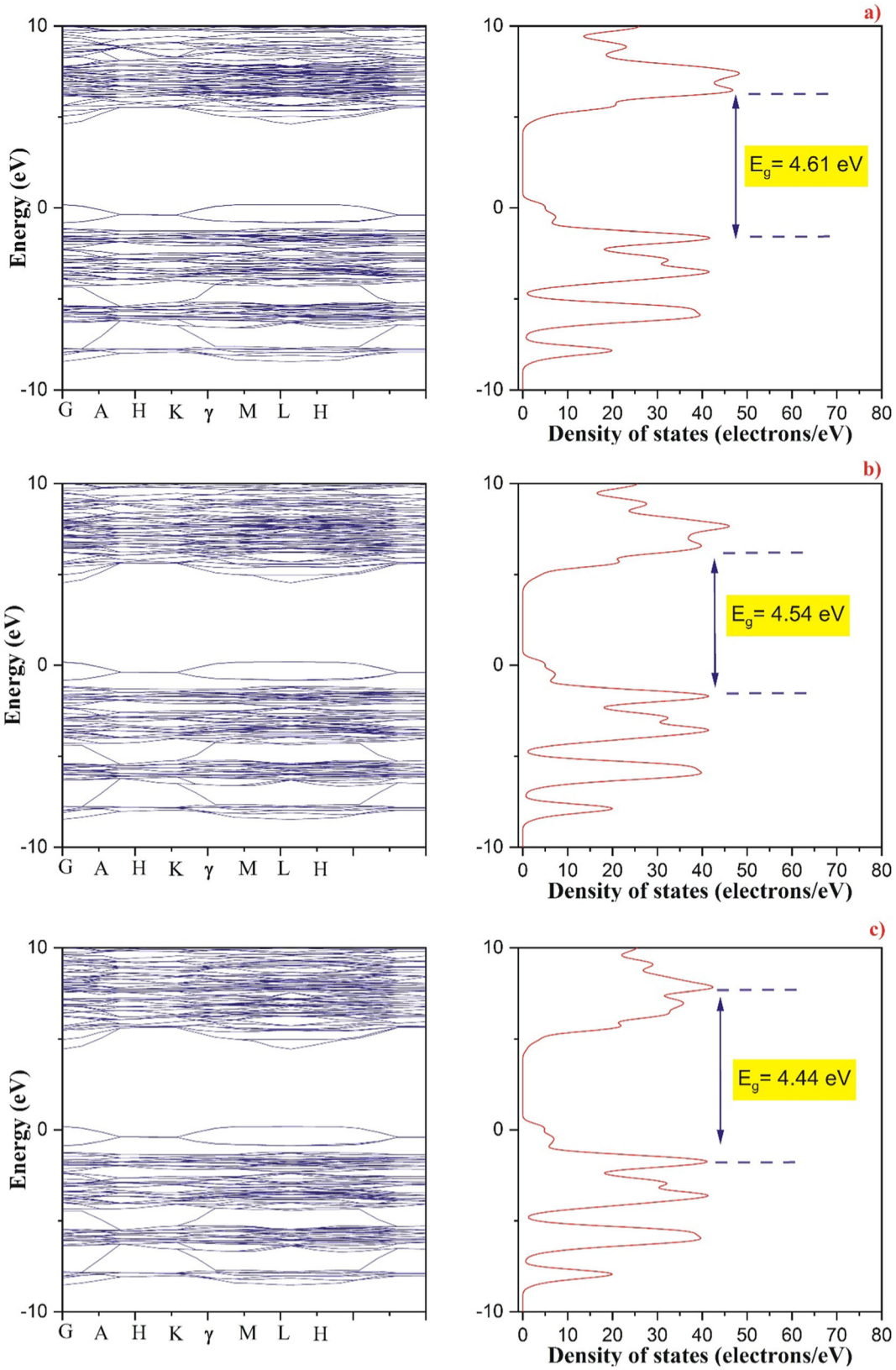

Fig. 4 The BS and DOS of the **a** 0.4Zn-HAp, **b** 0.4Zn–0.4 Mg-HAp, **c)** 0.4Zn–0.8 Mg-HAp, **d** 0.4Zn–1.2 Mg-HAp, **e** 0.4Zn–1.6 Mg-HAp, and **f** 0.4Zn–2.0 Mg-HAp

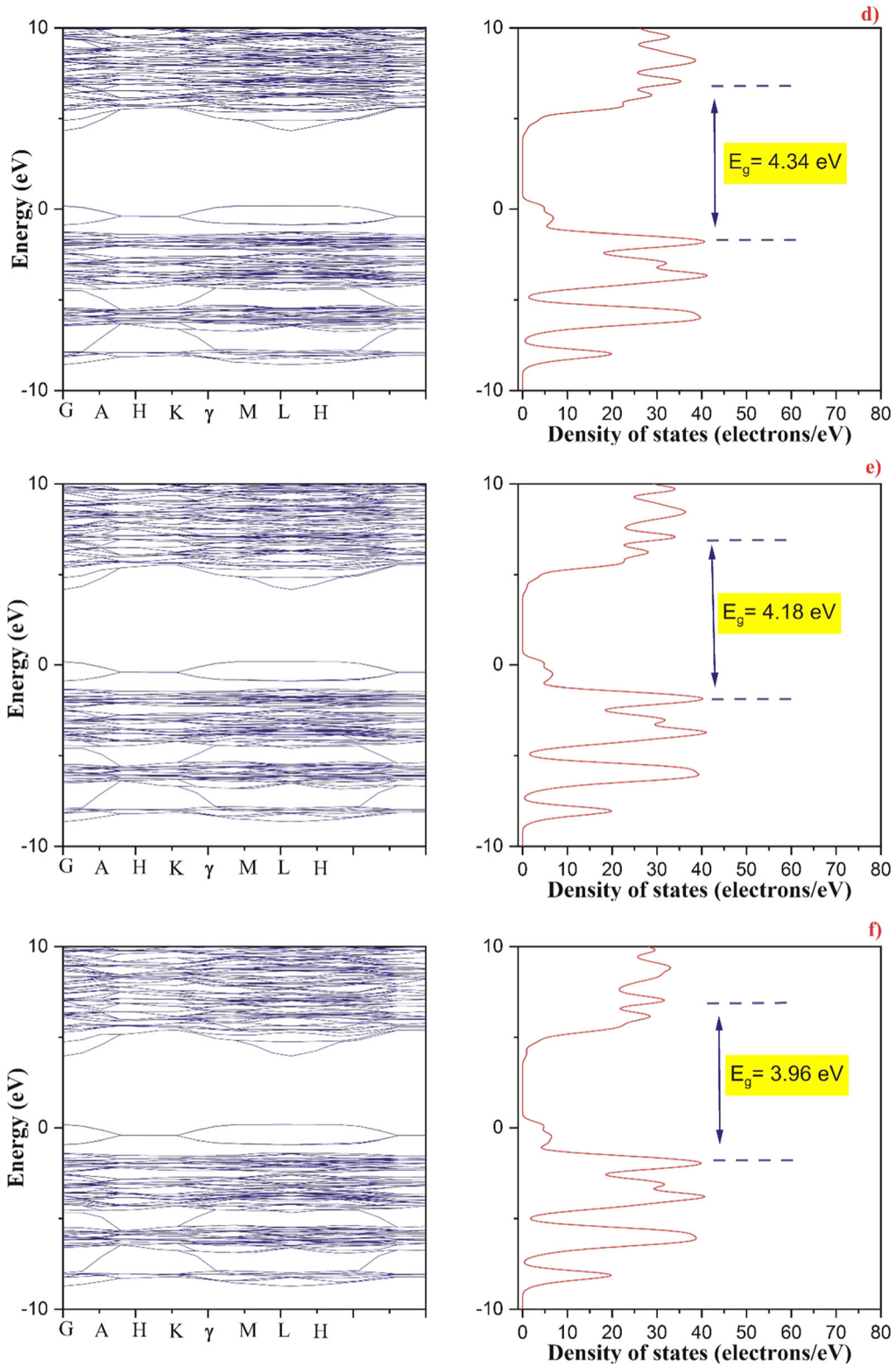

Fig. 4 continued

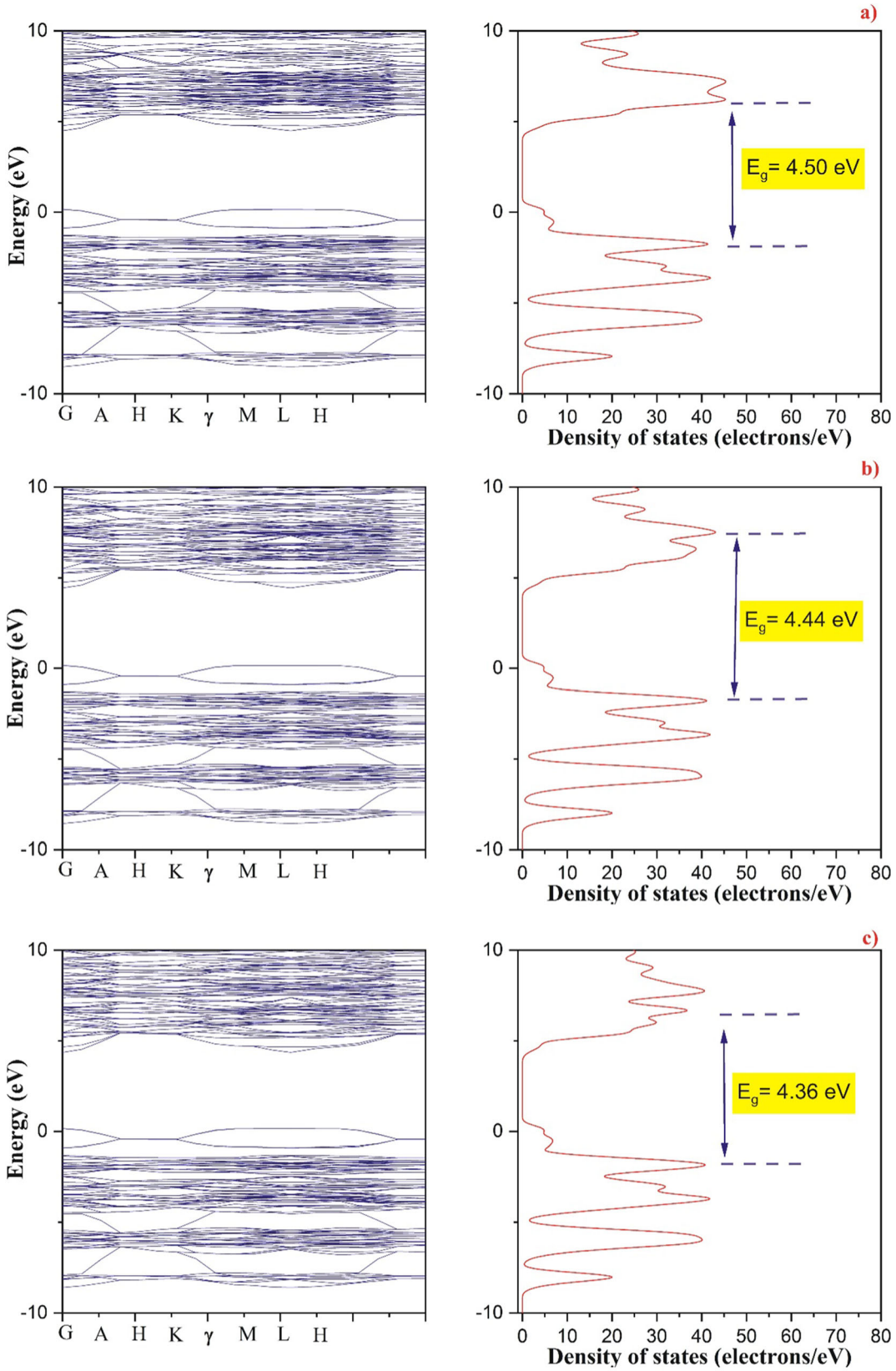

Fig. 5 The BS and DOS of the **a** 0.8Zn-HAp, **b** 0.8Zn–0.4 Mg-HAp, **c)** 0.8Zn–0.8 Mg-HAp, **d** 0.8Zn–1.2 Mg-HAp, **e)** 0.8Zn–1.6 Mg-HAp, and **f** 0.8Zn–2.0 Mg-HAp

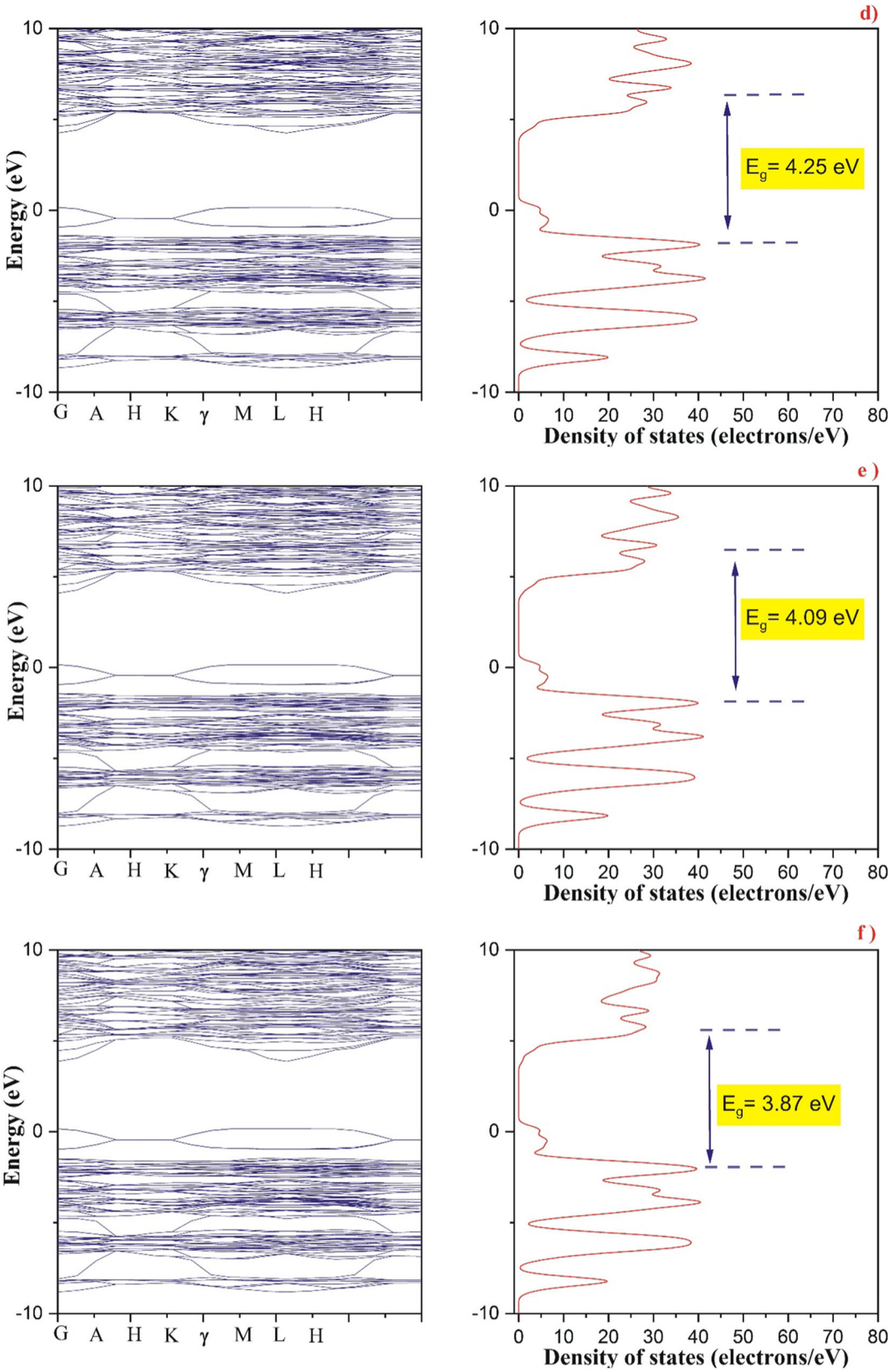

Fig. 5 continued

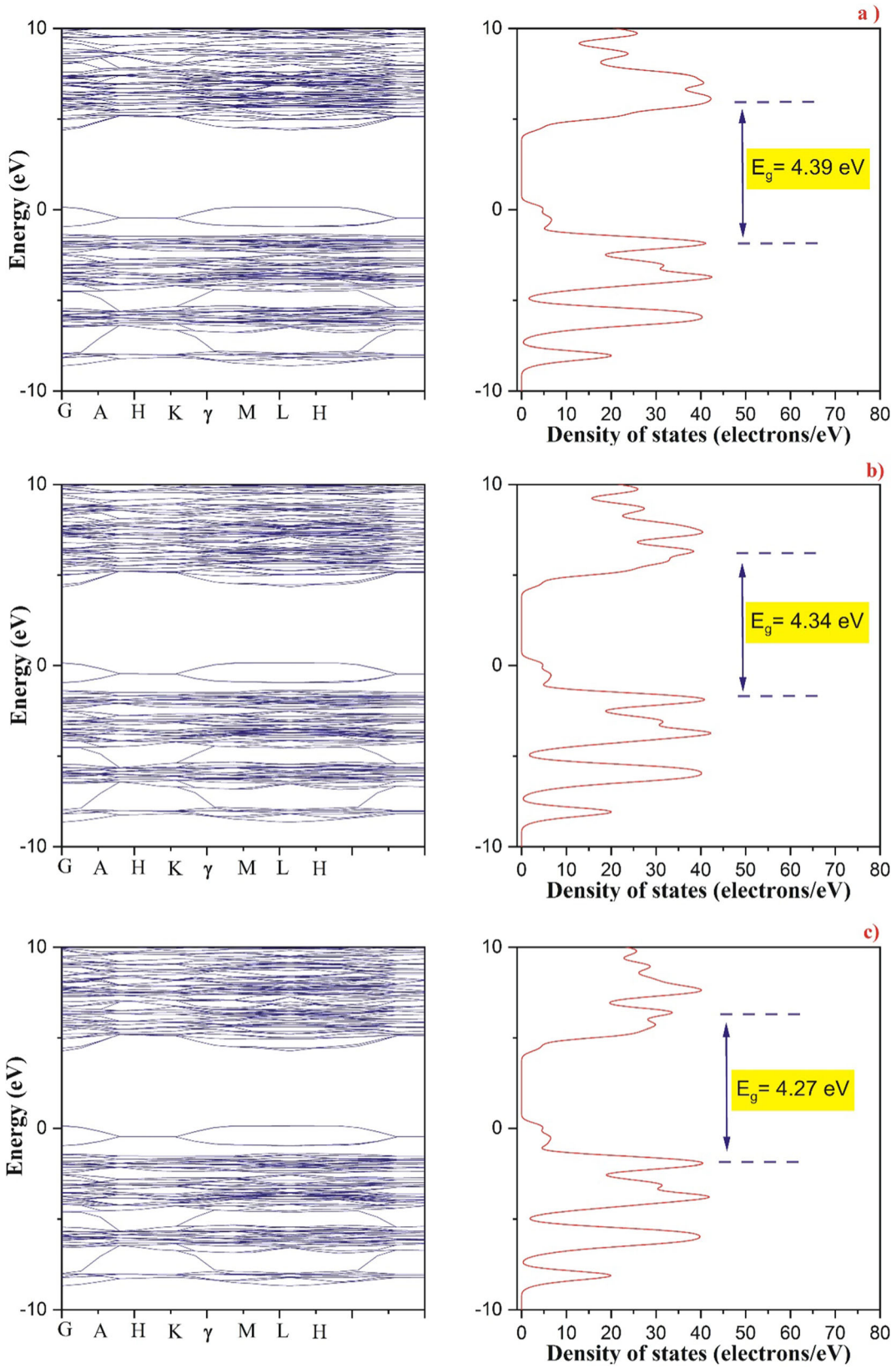

Fig. 6 The BS and DOS of the **a** 1.2Zn-HAp, **b** 1.2Zn–0.4 Mg-HAp, **c** 1.2Zn–0.8 Mg-HAp, **d** 1.2Zn–1.2 Mg-HAp, **e** 1.2Zn–1.6 Mg-HAp, and **f** 1.2Zn–2.0 Mg-HAp

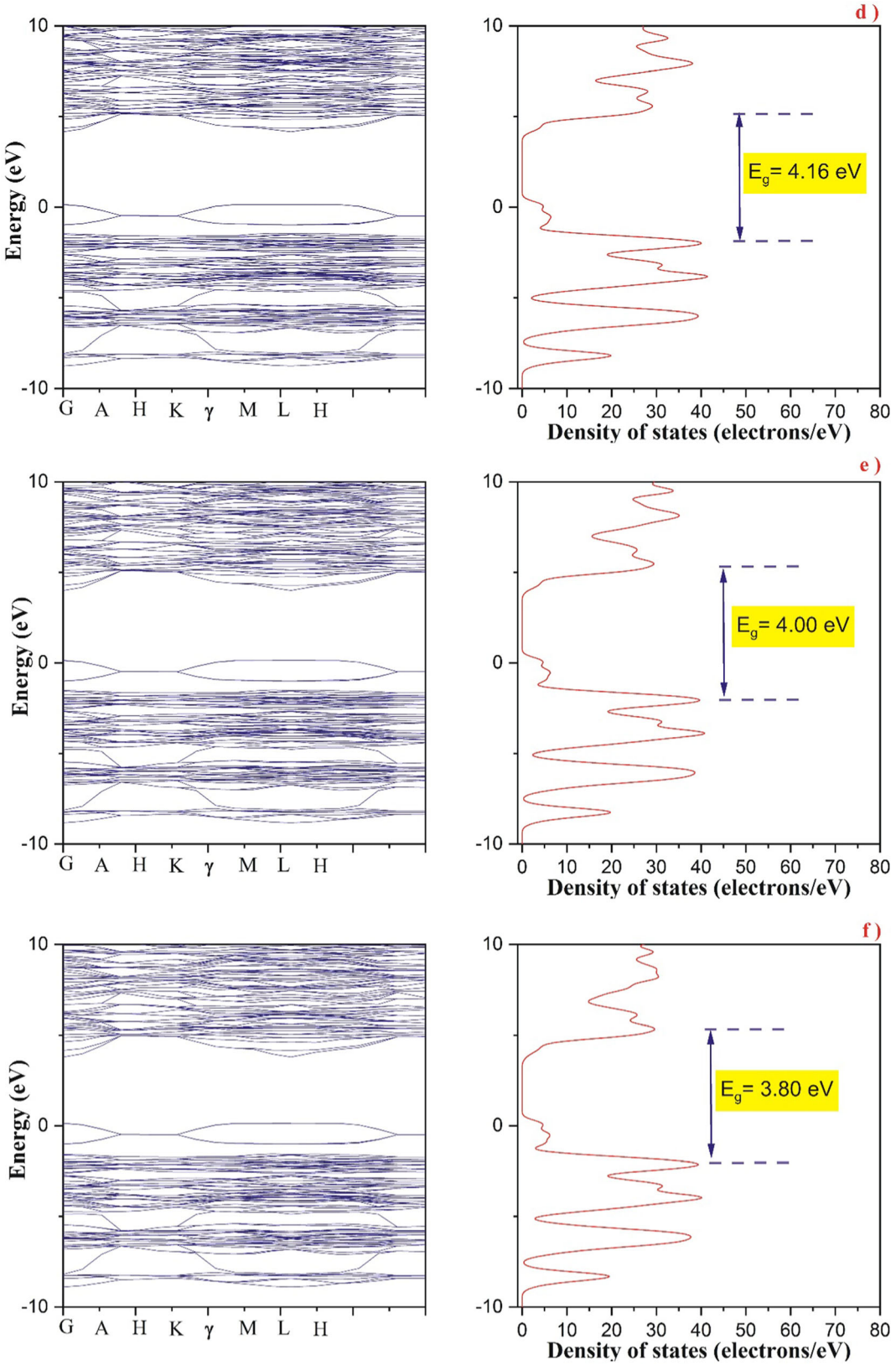

Fig. 6 continued

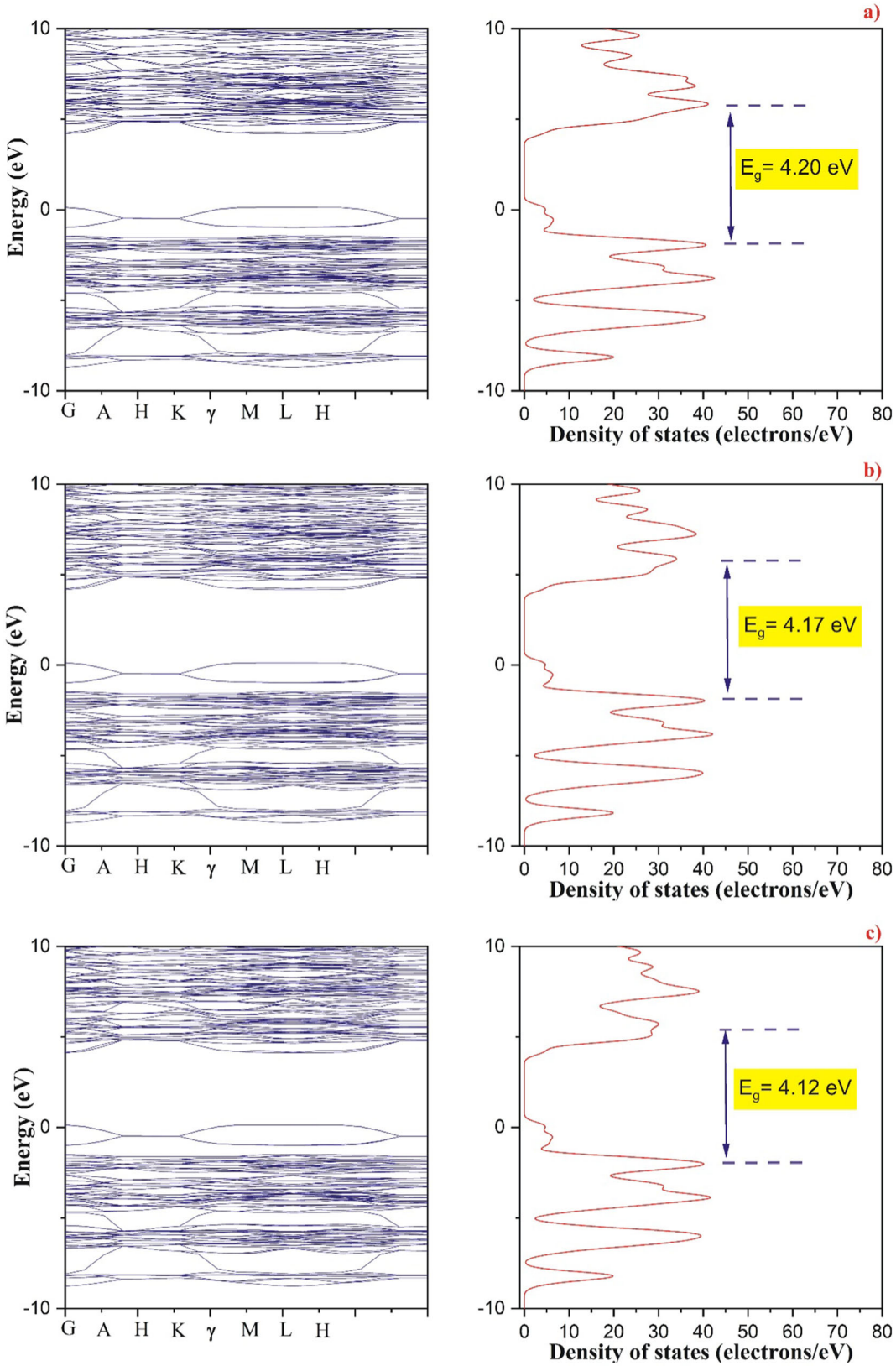

Fig. 7 The BS and DOS of the **a** 1.6Zn-HAp, **b** 1.6Zn–0.4 Mg-HAp, **c** 1.6Zn–0.8 Mg-HAp, **d** 1.6Zn–1.2 Mg-HAp, **e** 1.6Zn–1.6 Mg-HAp, and **f** 1.6Zn–2.0 Mg-HAp

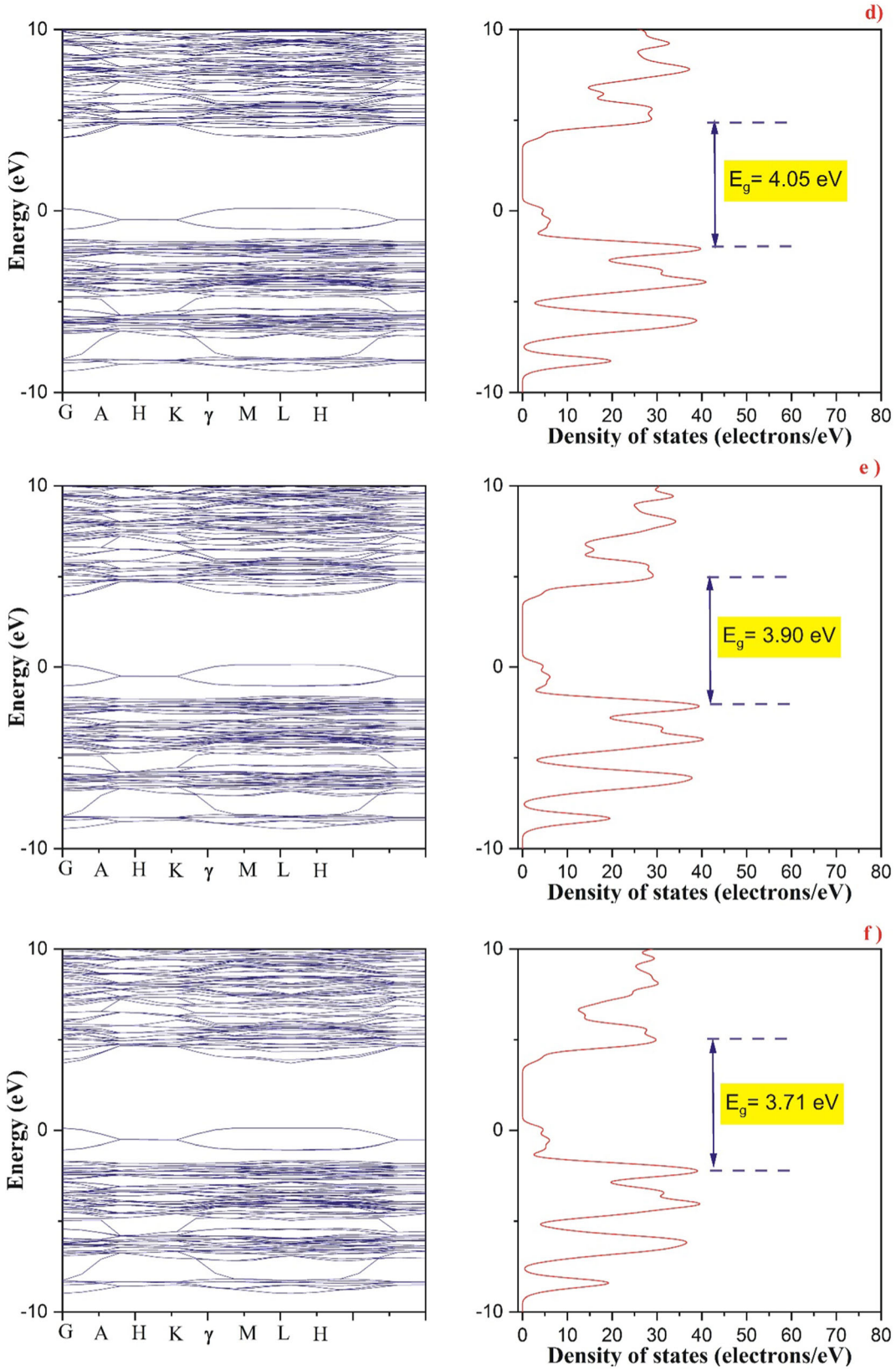

Fig. 7 continued

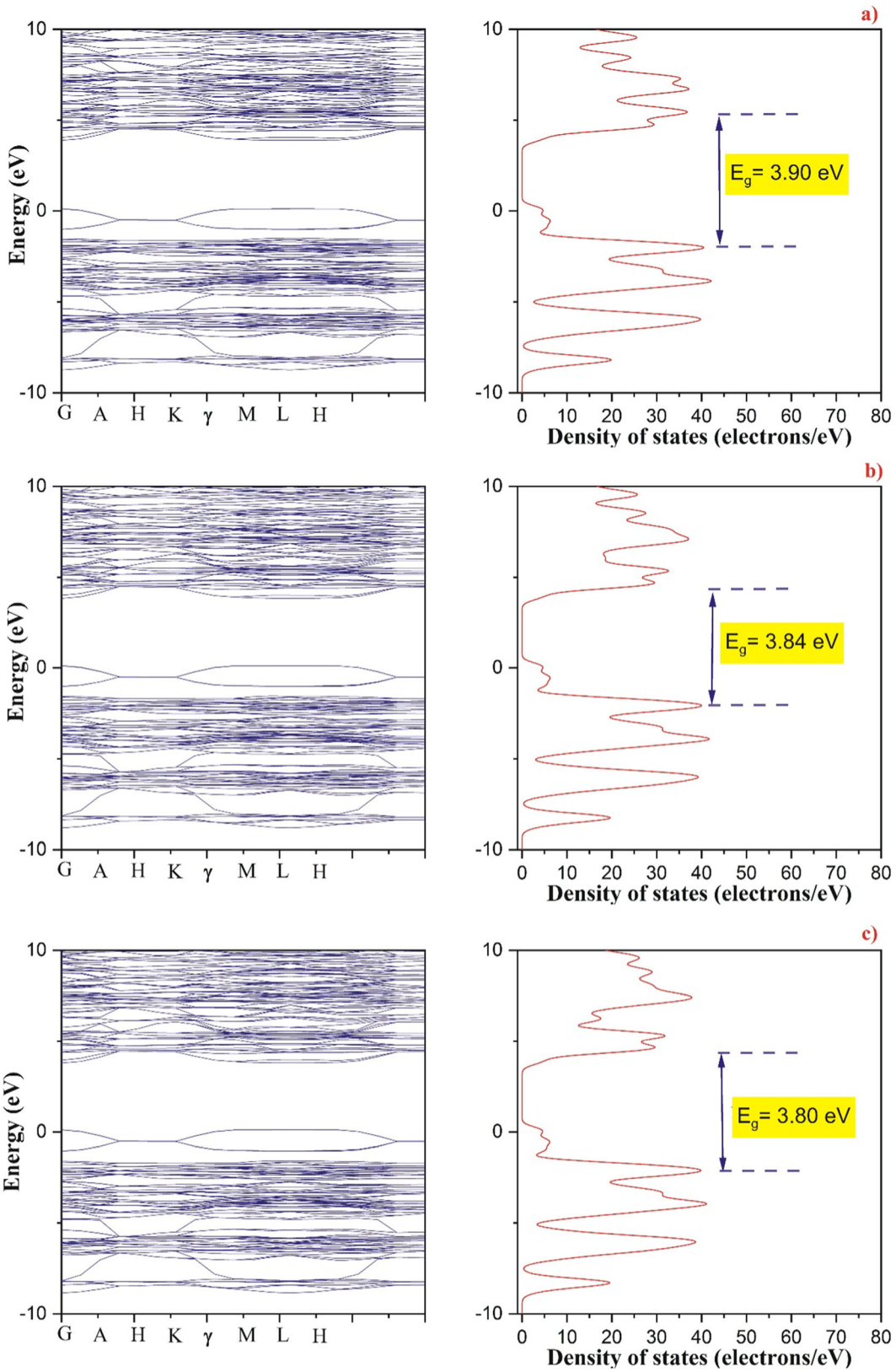

Fig. 8 The BS and DOS of the **a** 2.0Zn-HAp, **b** 2.0Zn–0.4 Mg-HAp, **c** 2.0Zn–0.8 Mg-HAp, **d** 2.0Zn–1.2 Mg-HAp, **e** 2.0Zn–1.6 Mg-HAp, and **f** 2.0Zn–2.0 Mg-HAp

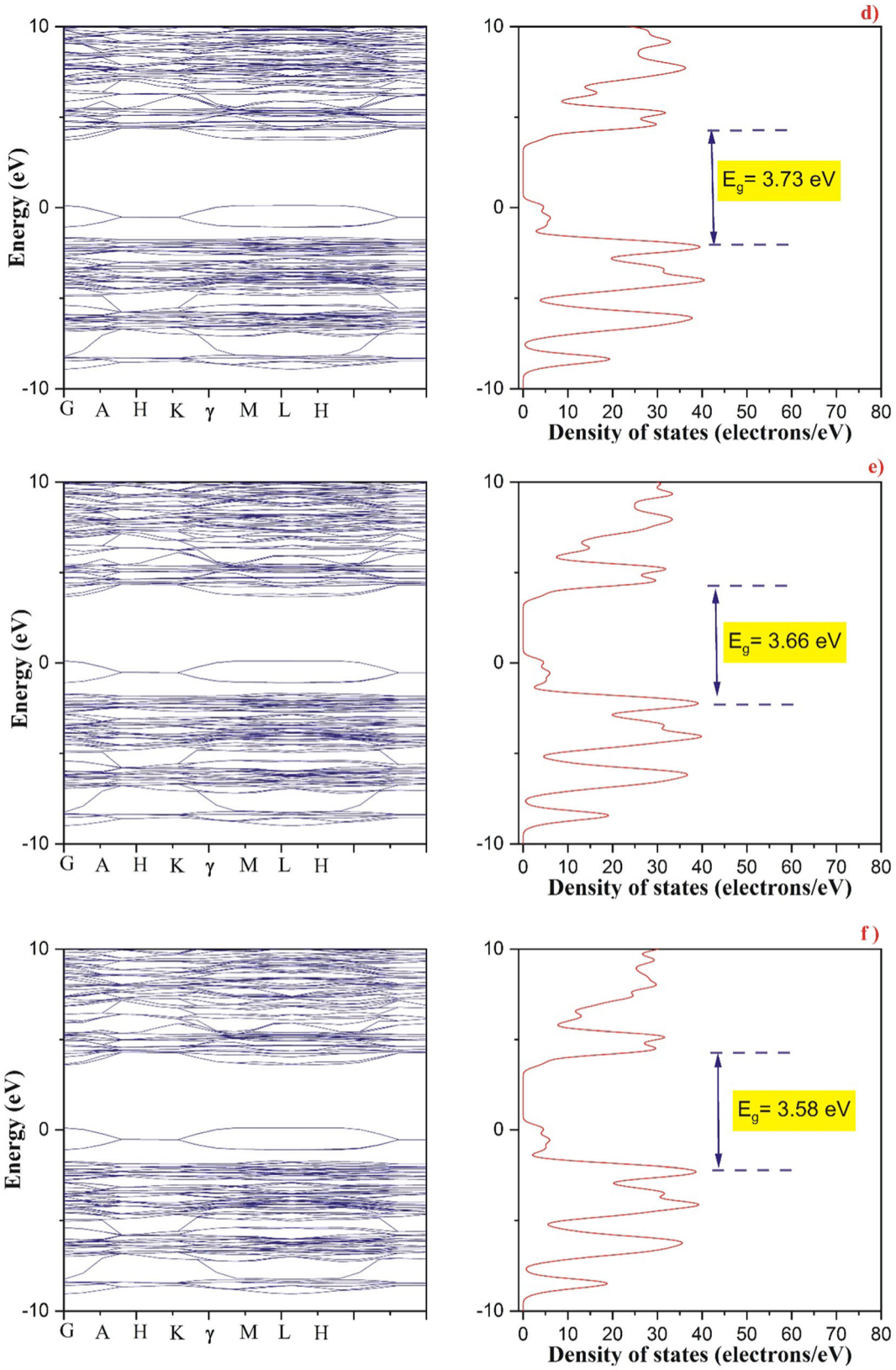

Fig. 8 continued

Table 1 Theoretical calculation results for Zn-based HAp structures doped with Mg

Structure	E_g (eV)	a (nm)	c (nm)	V (nm)^3	ρ (g cm^{-3})
0.4Zn-HAp	4.61	0.9357	0.6791	0.5149	3.158
0.4Zn–0.4 Mg-HAp	4.54	0.9349	0.6793	0.5142	3.156
0.4Zn–0.8 Mg-HAp	4.44	0.9349	0.6780	0.5132	3.154
0.4Zn–1.2 Mg-Hap	4.34	0.9330	0.6783	0.5113	3.152
0.4Zn–1.6 Mg-HAp	4.18	0.9312	0.6777	0.5089	3.150
0.4Zn–2.0 Mg-HAp	3.96	0.9305	0.6764	0.5072	3.148
0.8Zn-HAp	4.50	0.9351	0.6789	0.5141	3.161
0.8Zn–0.4 Mg-HAp	4.44	0.9346	0.6784	0.5132	3.159
0.8Zn–0.8 Mg-HAp	4.36	0.9329	0.6788	0.5116	3.157
0.8Zn–1.2 Mg-HAp	4.25	0.9315	0.6782	0.5096	3.155
0.8Zn–1.6 Mg-HAp	4.09	0.9306	0.6774	0.5080	3.153
0.8Zn–2.0 Mg-HAp	3.87	0.9298	0.6763	0.5063	3.151
1.2Zn-HAp	4.39	0.9343	0.6786	0.5130	3.164
1.2Zn–0.4 Mg-HAp	4.34	0.9337	0.6783	0.5121	3.162
1.2Zn–0.8 Mg-HAp	4.27	0.9322	0.6782	0.5104	3.160
1.2Zn–1.2 Mg-HAp	4.16	0.9311	0.6775	0.5087	3.158
1.2Zn–1.6 Mg-HAp	4.00	0.9302	0.6765	0.5069	3.156
1.2Zn–2.0 Mg-HAp	3.80	0.9284	0.6763	0.5048	3.154
1.6Zn-HAp	4.20	0.9331	0.6786	0.5117	3.168
1.6Zn–0.4 Mg-HAp	4.17	0.9320	0.6782	0.5102	3.166
1.6Zn–0.8 Mg-HAp	4.12	0.9313	0.6778	0.5091	3.164
1.6Zn–1.2 Mg-HAp	4.05	0.9304	0.6773	0.5077	3.162
1.6Zn–1.6 Mg-HAp	3.90	0.9293	0.6765	0.5059	3.160
1.6Zn–2.0 Mg-HAp	3.71	0.9279	0.6759	0.5040	3.158
2.0Zn-HAp	3.90	0.9325	0.6777	0.5103	3.171
2.0Zn–0.4 Mg-HAp	3.84	0.9309	0.6783	0.5090	3.169
2.0Zn–0.8 Mg-HAp	3.80	0.9304	0.6777	0.5080	3.167
2.0Zn–1.2 Mg-HAp	3.73	0.9294	0.6772	0.5066	3.165
2.0Zn–1.6 Mg-HAp	3.66	0.9280	0.6764	0.5044	3.163
2.0Zn–2.0 Mg-HAp	3.58	0.9265	0.6761	0.5026	3.161

to improve medical imaging (Jain et al. 2008). Besides, to create an antimicrobial activity, pure HAp was doped with Cu and Zn (Chen et al. 2010). In earlier works, HAp was doped with different ions such as Mn^{2+}, Ni^{2+}, K^{+}, Ag^{+}, Na^{+}, Cu^{2+}, Co^{2+}, Sr^{2+}, Ba^{2+}, Zn^{2+}, Mg^{2+}, Pb^{2+}, Cd^{2+}, Y^{3+}, La^{3+}, Ce^{3+}, Al^{3+}, F^{-}, Cl^{-}, Br^{-}, and CO_3^{2-} (Kaygili et al. 2013; Wopenka and Pasteris 2005; Clara et al. 2007; Hall et al. 1999; Peretz et al. 2001; Kanchana and Sekar 2010; Chen and Miao 2005; Eslami et al. 2008). All these ions can substitute Ca^{2+}, PO_4^{3-}, and OH^{-} ions within the crystalline lattice of HAp, which causes remarkable changes in its biological and mechanical properties. Zn and Ag have been used to improve the antimicrobial properties of the as-produced material (Chen et al. 2010; Gamal et al. 2023; El-Bassuony et al. (2023)).

However, the types and extents of ionic substitutions are difficult to comprehend owing to the complexity of the apatite crystal structure. In contrast, computer simulation provides an effective method for investigating various ion-doped HAps to understand both the substitution mechanisms and the characteristics of doping ions (Mostafa and Brown 2007). In general, ions-doped HAp has been studied using density functional theory (DFT).

DFT is a quantum mechanics (QM) method that studies the electronic structure characteristics of the ions doped in HAp. It does not require empirical parameters because it considers the system's total energy as a function of electron density (Mostafa and Brown 2007). The known findings on computer simulations of various single anion- and cation-doped HAps are summarized in Tables 2 and 3 of Ref. (Wang et al. 2017). Besides, DFT analysis has been performed on a number of ionic pairs co-doped into the HAp crystal lattice, including Si/Mg, Zr/Mg, Zn/Mg, Ag/Mg, and Sr/Mg co-doped HAps, which were synthesized using various techniques (Kim et al. 2003; Kaygili and Keser 2016; Alioui et al. 2019; Mosaad et al. 2023).

Furthermore, a survey on the Scopus database based on the growing interest in the electrical properties of HAp in the last decade has been shown as a bar chart figure in Ref. (Das and Pamu 2019). The figure compares the number of articles published in the recent decade (2007–2017) on biomaterial preparation versus the electrical properties of such biomaterials. A logical analysis of the electrical properties is essential for medical diagnosis and sensor-based uses of such materials and helps understand tissue and cell structures and functions. As is general knowledge, the desire for superior practical applications drives the need for greater system performance, which often involves energy gap, carrier mobility, etc. Even so, understanding the fundamentals of electrical behaviors/properties is the basis for the answers. Therefore, Eg is a key factor in determining its electrical conductivity. Additionally, the band structure and density of states (DOS) have a significant impact on how distinct materials' electronic properties are determined (Martin 2020). In order to comprehend the hidden scientific principles in the density distributions of free electrons in the metals, researchers in the domains of solid-state and condensed matter physics carefully analyze these distributions (Nørskov et al. 2009) and also to develop new materials (Seo et al. 2014; Ma et al. 2015). Recently, in our reported data for the first time the band structure, DOS and BG were computed for Sm/Mg, Sm/Zn, and Sm/Sr co-doped HAp to show the effect of the co-dopants with various rates on these samples' electronic properties (Hssain et al. 2022a, 2022b, 2022c).

This study aims to search band structures and DOS of five different group samples of Zn-doped HAp with additional doping with Mg at varying amounts. Several group of samples of Zn-containing HAps at a constant amount of 0.4, 0.8, 1.2, 1.6, and 2.0 at. % Zn were prepared and, in addition, the second dopant of Mg was utilized at varying amounts of 0.4, 0.8, 1.2, 1.6, and 2.0 at. %, for each group. To show the effects of dopants on the structural and electronic properties of all samples in each group, the lattice parameters of hexagonal co-doped HAp are obtained as well as band structure and DOS.

2 Materials and Methods

Previous studies from our group (Hssain et al. 2022a, 2022b, 2022c) have more thorough information on the density of states (DOS). DOS calculations can be obtained as

$$\mathrm{DOS(E)} = \sum \mathrm{g(E - \varepsilon_i)} \quad (1)$$

where g is a Gaussian function with a specified full-width-at-half-maximum, the total energy of a molecule is denoted by E, while the energy of its ith molecular orbital is denoted by ε_i. Samples were prepared at a predetermined rate, and potential of the system was obtained in our case. By using the CASTEP software, band structures have been calculated.

In DFT, the valence band states represent the electron energy levels that are occupied by valence electrons. These states originate from the atomic orbitals of the constituent elements in the crystal lattice. DFT calculates the electronic wave functions and energies associated with these states. It allows us to understand how electrons are distributed among the atoms in the crystal, leading to the formation of valence band states. The character and energy levels of these states provide insights into the chemical bonding and electronic properties of the material.

3 Results and Discussion

3.1 Band Gap and Density of States (DOS) Results

To make a good comparison between the un-doped HAp and doped HAps, the band structure and density of states belonging to the pure HAp are shown in Fig. 2a and b, respectively. The as-optimized structure with the higher co-dopants contents (2.0Zn–2.0 Mg-HAp), as an example, is shown in Fig. 3. Bandgaps (BG) for all selected sample groups are shown in Fig. 4a–f, 5a–f, 6a–f, 7a–f, and 8a–f, which are located in the interval points between (M−H). A continuous spectrum bench is present at both low and high energies. It appears that the valence and conduction band structures are flat. The highest occupied valence band and the lowest vacant conduction band are found in (M−H) points, demonstrating that a direct BG may be used to characterize these materials. Pure HAp, on the other hand, has an indirect BG. This is because the valence band's highest energy point occurs at different wave vectors $k = \gamma-\mathrm{K}$ or $\gamma-\mathrm{M}$, and the conduction band's lowest point is located at wave vector $k = \gamma$ (Avakyan et al. 2018). The BG energy of pure HAp was theoretically reported as 5.23 eV (Slepko and Demkov 2011), and its experimental value was determined to be 4.86 eV (Ignjatović et al. 2019). For the commercial HAp, this value was reported to be 4.92 eV (Bystrov et al. 2016). In another studies, this value was theoretically determined to be 5.08 eV (Moradi and Alvani 2020) and 4.71 eV (Mahmood et al. 2020). In this study, the results are more significant than previous work because the simulations are done for the five different sample groups of Zn-containing HAp with constant amounts for all samples of each group at of 0.4, 0.8, 1.2, 1.6, and 2.0 at. %, respectively, and co-doped with Mg at varying amounts for all samples that contains in each group

0.4, 0.8, 1.2, 1.6, and 2.0 at. %. The BG values were computed to be 4.61, 4.54, 4.44, 4.34, 4.18, and 3.96 eV for the first sample group of 0.4Zn-HAp, 0.4Zn–0.4 Mg-HAp, 0.4Zn–0.8 Mg-HAp, 0.4Zn–1.2 Mg-HAp, 0.4Zn–1.6 Mg-HAp, and 0.4Zn–2.0 Mg-HAp, respectively. Then, its values were found to be 4.50, 4.44, 4.36, 4.25, 4.09, and 3.87 eV for the second sample group of 0.8Zn-HAp, 0.8Zn–0.4 Mg-HAp, 0.8Zn–0.8 Mg-HAp, 0.8Zn–1.2 Mg-HAp, 0.8Zn–1.6 Mg-HAp, and 0.8Zn–2.0 Mg-HAp, respectively. Next, the values of this parameter were computed to be 4.39, 4.34, 4.27, 4.16, 4.00, and 3.80 eV for the third sample group of 1.2Zn-HAp, 1.2Zn–0.4 Mg-HAp, 1.2Zn–0.8 Mg-HAp, 1.2Zn–1.2 Mg-HAp, 1.2Zn–1.6 Mg-HAp, and 1.2Zn–2.0 Mg-HAp, respectively. After that, the calculated BG values were determined to be 4.20, 4.17, 4.12, 4.05, 3.90, and 3.71 eV for the fourth sample group of 1.6Zn-HAp, 1.6Zn–0.4 Mg-HAp, 1.6Zn–0.8 Mg-HAp, 1.6Zn–1.2 Mg-HAp, 1.6Zn–1.6 Mg-HAp, and 1.6Zn–2.0 Mg-HAp, respectively. Finally, this parameter's values were calculated to be 3.90, 3.84, 3.80, 3.723, 3.66, and 3.58 eV for the first sample group of 2.0Zn-HAp, 2.0Zn–0.4 Mg-HAp, 2.0Zn–0.8 Mg-HAp, 2.0Zn–2.0 Mg-HAp, 2.0Zn–1.6 Mg-HAp, and 2.0Zn–2.0 Mg-HAp, respectively. Consequently, as it can be seen from the aforementioned results that substitutions of Zn and Mg in the HAp lattice at various rates are important defects in it, which significantly affect the BG values of all sample groups as well as its electronic properties. The results obtained show that increasing the amount of the dopants in all sample groups has decreased considerably the BG energy. As shown in Table 1, the largest BG is found to be 4.61 eV for the sample of 0.4Zn-HAp which is a single (Zn) doped HAp with the smallest rate (0.4 at. %) in the first sample group. These largest values of BGs for the samples become remarkably smaller with increasing the amount of co-doped Mg of 0.8, 1.2, 1.6, and 2.0 at. %. Besides, with increase in the rates of Zn dopants in all sample groups, the BG value gradually reduced, and then, the highest amount of dopants in the sample of 2.0Zn–2.0 Mg-HAp leads to the smallest BG (3.58 eV) among all of the sample groups. In our prior studies, the increasing rates of used dopants of Er^{3+}, Sm^{3+}, Bi^{3+}, and Pr^{3+} (İsen et al. 2023; Kaygili et al. 2020; Kareem et al. 2022; Ahmed et al. 2023) had found to have a similar trend to lower BG levels. In addition, in our recent work, the same trends have been observed for decreasing the BG with increase in the amount of dopants for three different sample groups of Sm/Mg, Sm/Zn, and Sm/Sr co-doped HAp that investigated theoretically (Hssain et al. 2022a, 2022b, 2022c). Therefore, the results of this study highly agree with those of previous research. When electronic states change along axes of symmetry, the bandgap energy decreases, this can change the bandgap value due to doping.

When doping with foreign atoms like Mg, DFT allows us to investigate how the dopant atoms introduce new electronic states within the band structure. We can see the effect of it in the band structure figures.

3.2 Unit Cell Parameters and Density of the Zn and Mg co-Doped HAp Structures

The HAp structure for investigating how defects like ion substitutions affect its properties, is principally based on its initial, unaltered stoichiometric structural phase-hexagonal P63m, with a unit cell containing 44 atoms and consisting of structural OH channels with two hydroxyl OH groups in each unit cell (Bystrov et al. 2015; Bystrov 2017; Aronov et al. 2007). For each set of samples, we optimize the lattice parameters and generate the hexagonal supercells. The lattice parameters and the relaxed volumes of the supercells for all sample groups that modeled were found as shown in Table 1. The variations in the lattice parameters are predicted after the doping process with Zn constant rates and Mg at varying amounts for all samples in each group. It can be seen that the cell parameters and volume are decreased with increase in the amounts of dopants and thus the smallest cell parameters and volume are found to be 0.9265 nm, 0.6761 nm, and 0.5026 $(nm)^3$ for the sample 2.0Zn–2.0 Mg-HAp in the last group which includes the highest rates of both dopants among all of the samples of each group.

The theoretical density values have shown a significant result as gradually increased with the rising of the doping rates of Zn at constant values for each of the five different sample groups, thus the more Zn there are, the higher these values get. However, Mg at varying rates (0.4, 0.8, 1.2, 1.6, and 2.0 at. %) co-doped with Zn (at a constant amount for each group), which have decreased the density values gradually for each group, increasing the Zn doping from 0.4 to 2.0 at. % has shown a remarkable increase in the density values from the first group to the last one. According to Table, the sample of 0.4Zn–2.0 Mg-HAp has the lowest value of density to be 3.156 g cm^{-3} in the first group, while the highest value of density is belonged to the structure of 2.0Zn-HAp to be 3.171 g cm^{-3}. The higher amount of Zn causes the higher density, and the higher amount of Mg causes the lower density in each group. Ca, Mg, and Zn have known densities of 1.550, 1.738, and 7.133 g cm^{-3} (Apfelbaum 2017; Ibrahimzade et al. 2021), respectively. Since Zn and Mg ions have different densities that can be substituted for Ca ions, the change in density means that Mg and Zn ions occupy the places of Ca ions. Because the density of Mg ion is lower than that of Zn, high amount of Mg causes low density.

The higher amounts of both co-dopants are more effective in improving the electronic properties. The

addition of both co-dopants to the HAp structure contributes to its conduction mechanism. It affects its crystal structure-related parameters as mentioned above, but it should not be overlooked that a high amount of the additive(s) may be caused by the toxic effects (İsen et al. 2023; Kaygili et al. 2020; Kareem et al. 2022; Apfelbaum 2017).

4 Conclusion

The band structures and DOS of the Zn-based HAps were doped with Mg at various amounts. Zn and Mg contents affected the band structures, lattice parameters, DOS, and density. Adding Mg caused a gradual decrease in the parameters, including bandgap energy, density, lattice parameters, and unit cell volume. High levels of Zn caused the smaller values for band gap, lattice parameters, and unit cell volume, while the higher values for the density were observed. Significantly, it was seen that the amount of Zn was more effective in decreasing the band gap than Mg. Both elements can be used for controlling the parameters as mentioned above.

Author Contributions All authors contributed equally to this paper and read and approved the final manuscript.

Funding No funding was received for conducting this research work.

Data Availability No data were used to support this study.

Declarations

Conflict of interest No potential conflict of interest was reported by the authors.

References

Ahmed LO, Bulut N, Osmanlıoğlu F, Tatar B, Kebiroglu H, Ates T et al (2023) Theoretical and experimental investigation of the effects of Pr dopant on the electronic band structure, thermal, structural, in vitro biocompatibility of Er-based hydroxyapatites. J Mol Struct 1280:135095

Alioui H, Bouras O, Bollinger J-C (2019) Toward an efficient antibacterial agent: Zn-and Mg-doped hydroxyapatite nanopowders. J Environ Sci Health A 54:315–327. https://doi.org/10.1080/10934529.2018.1550292

Apfelbaum EM (2017) Calculation of thermophysical properties of titanium and zinc plasmas. High Temp 55:1–11. https://doi.org/10.1134/S0018151X16060018

Aronov D, Chaikina M, Haddad J, Karlov A, Mezinskis G, Oster L, Pavlovska I, Rosenman G (2007) Electronic states spectroscopy of Hydroxyapatite ceramics. J Mater Sci: Mater Med 18:865–870. https://doi.org/10.1007/s10856-006-0080-3

Avakyan LA, Paramonova EV, Coutinho J, Öberg S, Bystrov VS, Bugaev LA (2018) Optoelectronics and defect levels in hydroxyapatite by first-principles. J Chem Phys 148(15):154706

Badran H, Yahia I, Hamdy MS, Awwad N (2017) Lithium-doped hydroxyapatite nano-composites: synthesis, characterization, gamma attenuation coefficient and dielectric properties. Radiat Phys Chem 130:85–91. https://doi.org/10.1016/j.radphyschem.2016.08.001

Bhattacharjee A, Gupta A, Verma M, Murugan PA, Sengupta P, Matheshwaran S, Manna I, Balani K (2019) Site-specific antibacterial efficacy and cyto/hemo-compatibility of zinc substituted hydroxyapatite. Ceram Int 45:12225–12233. https://doi.org/10.1016/j.ceramint.2019.03.132

Bystrov VS (2017) Computational studies of the hydroxyapatite nanostructures, peculiarities and properties. Math Biol Bioinform 12:14–54. https://doi.org/10.17537/2017.12.14

Bystrov V, Coutinho J, Bystrova A, Dekhtyar YD, Pullar R, Poronin A, Palcevskis E, Dindune A, Alkan B, Durucan C (2015) Computational study of hydroxyapatite structures, properties and defects. J Phys D 48:195302. https://doi.org/10.1088/0022-3727/48/19/195302

Bystrov VS, Piccirillo C, Tobaldi DM, Castro PML, Coutinho J, Kopyl S, Pullar RC (2016) Oxygen vacancies, the optical band gap (Eg) and photocatalysis of hydroxyapatite: comparing modelling with measured data. Appl Catal B 196:100–107. https://doi.org/10.1016/j.apcatb.2016.05.014

Chen Y, Miao X (2005) Thermal and chemical stability of fluorohydroxyapatite ceramics with different fluorine contents. Biomaterials 26:1205–1210. https://doi.org/10.1016/j.biomaterials.2004.04.027

Chen Y, Zheng X, Xie Y, Ji H, Ding C, Li H, Dai K (2010) Silver release from silver-containing hydroxyapatite coatings. Surf Coat Technol 205:1892–1896. https://doi.org/10.1016/j.surfcoat.2010.08.073

Clara M, Magalhães F, Williams PA (2007) Apatite group minerals: solubility and environmental remediation. In: Letcher TM (ed) Thermodynamics, solubility and environmental issues. Elsevier, London, p 327

Coelho CC, Araújo R, Quadros PA, Sousa SR, Monteiro FJ (2019) Antibacterial bone substitute of hydroxyapatite and magnesium oxide to prevent dental and orthopaedic infections. Mater Sci Eng C 97:529–538. https://doi.org/10.1016/j.msec.2018.12.059

Das A, Pamu D (2019) A comprehensive review on electrical properties of hydroxyapatite based ceramic composites. Mater Sci Eng C 101:539–563. https://doi.org/10.1016/j.msec.2019.03.077

El-Bassuony AA, Abdelsalam HK (2023) Attractive study of the physical properties of silver iron oxide nanoparticles for biomedical applications. Physica Scripta 98(5):055919. https://doi.org/10.1088/1402-4896/acc90c

Eslami H, Solati-Hashjin M, Tahriri M (2008) Synthesis and characterization of nanocrystalline fluorinated hydroxyapatite powder by modified wet-chemical process. J Ceram Process Res 9:224–229

Gamal WM, El-Bassuony AAH, Abdelsalam HK (2023) Fascinating study of elastic, FTIR, and antimicrobial properties of silver nanochromite at different annealing temperatures. Polym Bull. https://doi.org/10.1007/s00289-023-04788-4

Hall S, Dimai H, Farley J (1999) Effects of zinc on human skeletal alkaline phosphatase activity in vitro. Calcif Tissue Int 64:163–172. https://doi.org/10.1007/s002239900597

Hssain AH, Bulut N, Ates T, Koytepe S, Kuruçay A, Kebiroglu H, Kaygili O (2022a) Experimental characterization and theoretical investigation of Zn/Sm co-doped hydroxyapatites. Mater Today Commun 31:103850. https://doi.org/10.1016/j.mtcomm.2022.103850

Hssain AH, Bulut N, Ates T, Koytepe S, Kuruçay A, Kebiroglu H, Kaygili O (2022b) The experimental and theoretical

investigation of Sm/Mg co-doped hydroxyapatites. Chem Phys Lett 800:139677. https://doi.org/10.1016/j.cplett.2022.139677
Hssain AH, Bulut N, Ates T, Koytepe S, Kuruçay A, Kebiroglu H, Kaygili O (2022c) Sr/Smco-doped hydroxyapatites: experimental characterization and theoretical research. J Aust Ceram Soc 58:1491–1507. https://doi.org/10.1007/s41779-022-00788-1
Ibrahimzade L, Kaygili O, Dundar S, Ates T, Dorozhkin SV, Bulut N, Koytepe S, Ercan F, Gürses C, Hssain AH (2021) Theoretical and experimental characterization of Pr/Ce co-doped hydroxyapatites. J Mol Struct 1240:130557. https://doi.org/10.1016/j.molstruc.2021.130557
Ignjatović NL, Mančić L, Vuković M, Stojanović Z, Nikolić MG, Škapin S, Jovanović S, Veselinović L, Uskoković V, Lazić S, Marković S (2019) Rare-earth (Gd3+, Yb3+/Tm3+, Eu3+) co-doped hydroxyapatite as magnetic, up-conversion and down-conversion materials for multimodal imaging. Sci Rep 9(1):16305
İsen F, Kaygili O, Bulut N, Ates T, Osmanlıoğlu F, Keser S et al (2023) Experimental and theoretical characterization of Dy-doped hydroxyapatites. J Aust Ceram Soc. https://doi.org/10.1007/s41779-023-00878-8
Jain TK, Richey J, Strand M, Leslie-Pelecky DL, Flask CA, Labhasetwar V (2008) Magnetic nanoparticles with dual functional properties: drug delivery and magnetic resonance imaging. Biomaterials 29:4012–4021. https://doi.org/10.1016/j.biomaterials.2008.07.004
Kanchana P, Sekar C (2010) Influence of sodium fluoride on the synthesis of hydroxyapatite by gel method. J Cryst Growth 312:808–816. https://doi.org/10.1016/j.jcrysgro.2009.12.032
Kareem RO, Kaygili O, Ates T, Bulut N, Koytepe S, Kuruçay A et al (2022) Experimental and theoretical characterization of Bi-based hydroxyapatites doped with Ce. Ceram Int 48:33440–33454
Kaygili O, Keser S (2016) Zr/Mg, Zr/Sr and Zr/Zn co-doped hydroxyapatites: synthesis and characterization. Ceram Int 42:9270–9273. https://doi.org/10.1016/j.ceramint.2016.02.027
Kaygili O, Keser S, Ates T, Al-Ghamdi AA, Yakuphanoglu F (2013) Controlling of dielectrical and optical properties of hydroxyapatite based bioceramics by Cd content. Powder Technol 245:1–6. https://doi.org/10.1016/j.powtec.2013.04.012
Kaygili O, Keser S, Ates T, Tatar C, Yakuphanoglu F (2015) Controlling of dielectric parameters of insulating hydroxyapatite by simulated body fluid. Mater Sci Eng C 46:118–124. https://doi.org/10.1016/j.msec.2014.10.024
Kaygili O, Vural G, Keser S, Yahia IS, Bulut N, Ates T et al (2020) Ce/Sm co-doped hydroxyapatites: synthesis, characterization, and band structure calculation. J Aust Ceram Soc 57:305–317
Kim S, Lee J, Kim Y, Riu D-H, Jung S, Lee Y, Chung S, Kim Y (2003) Synthesis of Si, Mg substituted hydroxyapatites and their sintering behaviors. Biomaterials 24:1389–1398. https://doi.org/10.1016/S0142-9612(02)00523-9
Koutsopoulos S (2002) Synthesis and characterization of hydroxyapatite crystals: a review study on the analytical methods. J Biomed Mater Res 62:600–612. https://doi.org/10.1002/jbm.10280
Liao L, Yang S, Miron RJ, Wei J, Zhang Y, Zhang M (2014) In vitro characterization of PBLG-g-HA/PLLA nanocomposite scaffolds. J Wuhan Univ Technol Mater Sci Ed 29:841–847. https://doi.org/10.1007/s11595-014-1006-4
Ma X, Li Z, Achenie LE, Xin H (2015) Machine-learning-augmented chemisorption model for CO_2 electroreduction catalyst screening. J Phys Chem Lett 6:3528–3533. https://doi.org/10.1021/acs.jpclett.5b01660
Mahmood BK, Kaygili O, Bulut N, Dorozhkin SV, Ates T, Koytepe S et al (2020) Effects of strontium - erbium co-doping on the structural properties of hydroxyapatite: an experimental and theoretical study. Ceram Int 46:16354–16363
Martin RM (2020) Electronic structure: basic theory and practical methods. Cambridge University Press, Cambridge
Moradi K, Alvani AS (2020) First-principles study on Sr-doped hydroxyapatite as a biocompatible filler for photo-cured dental composites. J Aust Ceram Soc 56:591–598
Mosaad KE, Shoueir KR, Dewidar MM (2023) Fabrication of multifunctional wound dressing composite biomaterials composed of Ag/Mg-hydroxyapatite doped electrospun poly (vinyl alcohol) nanofibers for skin tissue regeneration. J Clust Sci 34:135–146. https://doi.org/10.1007/s10876-021-02195-1
Mostafa NY, Brown PW (2007) Computer simulation of stoichiometric hydroxyapatite: structure and substitutions. J Phys Chem Solids 68:431–437. https://doi.org/10.1016/j.jpcs.2006.12.011
Nørskov JK, Bligaard T, Rossmeisl J, Christensen CH (2009) Towards the computational design of solid catalysts. Nature Chem 1:37–46. https://doi.org/10.1038/nchem.121
Peretz A, Papadopoulos T, Willems D, Hotimsky A, Michiels N, Siderova V, Bergmann P, Neve J (2001) Zinc supplementation increases bone alkaline phosphatase in healthy men. J Trace Elem Med Biol 15:175–178. https://doi.org/10.1016/S0946-672X(01)80063-8
Perry DL (2011) Handbook of inorganic compounds. CRC Press
Seo D-H, Shin H, Kang K, Kim H, Han SS (2014) First-principles design of hydrogen dissociation catalysts based on isoelectronic metal solid solutions. J Phys Chem Lett 5:1819–1824. https://doi.org/10.1021/jz500496e
Slepko A, Demkov AA (2011) First-principles study of the biomineral hydroxyapatite. Phys Rev B 84(13):134108
Sun L, Guo D, Zhao W, Wang L, Xu K (2014) Influences of reaction parameters and Ce contents on structure and properties of nano-scale Ce-HA powders. J Mater Sci Technol 30:776–781. https://doi.org/10.1016/j.jmst.2014.06.001
Ullah I, Li W, Lei S, Zhang Y, Zhang W, Farooq U, Ullah S, Ullah MW, Zhang X (2018) Simultaneous co-substitution of Sr^{2+}/Fe^{3+} in hydroxyapatite nanoparticles for potential biomedical applications. Ceram Int 44:21338–21348. https://doi.org/10.1016/j.ceramint.2018.08.187
Wang M, Wang Q, Lu X, Wang K, Ren F (2017) Computer simulation of ions doped hydroxyapatite: a brief review. J Wuhan Univ Technol Mater Sci Ed 32:978–987. https://doi.org/10.1007/s11595-017-1699-2
Wopenka B, Pasteris JD (2005) A mineralogical perspective on the apatite in bone. Mater Sci Eng C 25:131–143. https://doi.org/10.1016/j.msec.2005.01.008
Yin M, Xu W, Cui B, Dai H, Han Y, Yin Y, Li S (2014) Effects of the interaction between hydroxyapatite nanoparticles and hepatoma cells. J Wuhan Univ Technol Mater Sci Ed 29:635–642. https://doi.org/10.1007/s11595-014-0970-z